jove | Biochemistry

DATE PUBLISHED November 20, 2026
DOI 10.3791/74404
URL jove.com/t/74404

Microinjection-Based Single-Molecule Fluorescence Spectroscopy: Probing Protein Conformations and Dynamics in Live Cells

Yuhan Wang[1], **Daniel Nettels**[1], **Benjamin Schuler**[1,2]

[1]Department of Biochemistry, University of Zurich [2]Department of Physics, University of Zurich

Corresponding Authors : Yuhan Wang <y.wang@bioc.uzh.ch>, Benjamin Schuler <schuler@bioc.uzh.ch>

Citation

Wang, Y., Nettels, D., Schuler, B. Microinjection-Based Single-Molecule Fluorescence Spectroscopy: Probing Protein Conformations and Dynamics in Live Cells. *J. Vis. Exp.* (237), e74404, doi:10.3791/74404. (2026).

Abstract

Single-molecule fluorescence spectroscopy is a powerful approach for studying biomolecular conformations and dynamics with high sensitivity and quantitative precision, especially combined with Förster resonance energy transfer (FRET). When applied to live cells, however, measuring individual molecules in the complex intracellular environment remains technically challenging, particularly because efficient delivery, cell viability, fluorescence imaging, and data acquisition must be carefully coordinated. Here, the authors present a protocol for introducing fluorescently labeled proteins of interest into individual living eukaryotic cells by microinjection, followed by fluorescence imaging and time-resolved single-molecule data acquisition. This approach enables subcellularly resolved measurements of molecular diffusion, conformations, and dynamics in live cells. Representative measurements of donor-acceptor-labeled prothymosin α in HeLa cells illustrate the analysis of protein conformation by FRET, translational diffusion by fluorescence correlation spectroscopy, and rapid chain dynamics by nanosecond fluorescence correlation spectroscopy using time-tagged photon data. The protocol provides a versatile platform for investigating biomolecular mechanisms under native intracellular conditions and can be adapted to diverse molecular systems and cell types.

Introduction

Proteins are dynamic molecules that populate conformational ensembles rather than remaining in a single static structure. Transitions within these ensembles are central to protein folding, recognition, catalysis, regulation, and interaction[1,2,3,4,5,6]. However, protein behavior measured in dilute buffer solutions *in vitro* does not necessarily reproduce that in a cell, where macromolecular crowding, high viscosity, complex interactions with cellular structures, spatial confinement, metabolites, and specific or nonspecific binding partners can alter conformational equilibria and dynamics[7,8,9,10,11,12]. These effects can be particularly pronounced for intrinsically disordered proteins (IDPs), whose dimensions and dynamics are highly responsive to their surroundings owing to the lack of well-defined tertiary structure[13,14,15]. Consequently, understanding how proteins function under physiological conditions requires methods that can probe their conformations and dynamics directly in living cells.

Several experimental approaches provide complementary information about proteins in cellular environments. Fluorescence imaging reveals localization, redistribution, and interactions with high spatial and temporal resolution[8,16]. Ensemble FRET and fluorescence lifetime imaging can report average changes in molecular proximity or conformation[17], but these often cannot resolve conformational or dynamic heterogeneity. In-cell nuclear magnetic resonance (NMR) spectroscopy can provide residue-specific information about protein structure, dynamics, and

Copyright © 2026, Journal of Visualized Experiments
Creative Commons Attribution-NonCommercial-NoDerivs 3.0 Unported License

DOI 10.3791/74404

interactions[18,19], but its application is constrained by sensitivity and the correspondingly high intracellular concentrations required, and spectral broadening. Cryo-electron tomography can visualize macromolecular structures and assemblies in a near-native state at high spatial resolution in the cellular environment[20], but the cryogenic conditions prevent dynamics from being monitored directly. Thus, despite substantial methodological progress, obtaining quantitative, time-resolved information about heterogeneous protein conformations and dynamics at defined locations within living cells remains challenging[21,22].

Confocal single-molecule fluorescence spectroscopy provides a complementary approach with high sensitivity and broad temporal coverage[21,23,24]. As individual freely diffusing, fluorescently labeled molecules pass through the confocal observation volume, they generate photon bursts that can be analyzed individually. Single-molecule Förster resonance energy transfer (smFRET) provides distance-sensitive information about conformational distributions and allows coexisting molecular populations to be distinguished without ensemble averaging[23,24]. Alternating-laser excitation (ALEX) and pulsed interleaved excitation (PIE) enable donor-acceptor stoichiometry to be evaluated, while PIE additionally provides fluorescence lifetime information[25,26]. Fluorescence correlation spectroscopy (FCS) reports on fluctuations in fluorescence intensity and allows us to determine translational diffusion and molecular concentration[27], whereas nanosecond FCS (nsFCS) and related photon-statistical approaches provide access to rapid conformational dynamics, such as the submicrosecond chain reconfiguration typical of IDPs[28,29]. Together, these analyses can characterize molecular localization, diffusion, conformational heterogeneity, dynamics, assemblies, and biomolecular condensates, using the same time-tagged photon data[21,30].

Implementing these measurements in living eukaryotic cells requires several experimental aspects to be carefully coordinated[21,31,32,33]. Site-specifically dye-labeled proteins must be delivered into the cell without aggregation or loss of labeling quality. The intracellular concentration must be sufficiently low so that no more than one molecule occupies the confocal detection volume to ensure single-molecule detection while providing sufficiently many fluorescence bursts for quantitative analysis before all molecules are photobleached. Cell viability must be maintained throughout injection and acquisition, intracellular measurement positions must be selected accurately, and cellular autofluorescence, photobleaching, and time-dependent changes in background must be considered.

Several approaches have been used to introduce labeled molecules for intracellular smFRET. Electroporation enables parallel delivery of prelabeled molecules into many cells but offers less control over the amount introduced into individual cells and their subcellular localization[31,32,33]. Exogenous expression has enabled single-molecule FRET of genetically encoded GFP as a donor combined with HaloTag-based labeling with TMR as an acceptor[34], but it offers less control over intracellular concentration and labeling stoichiometry, introduces large fusion proteins, and can suffer from the inferior photophysical properties of fluorescent proteins compared to organic fluorophores. Streptolysin-O is a large bacterial pore that can be added to permeabilize eukaryotic cells and allow purified, organic-dye-labeled molecules to be introduced into cells, but it requires optimization of membrane permeabilization and recovery and does not directly target a specific compartment[35]. Although microinjection has lower throughput and requires specialized equipment and operator skill, it provides reproducible control over the amount introduced, minimizes the delay before measurement, preserves cell adherence, and allows purified proteins site-specifically labeled with optimal fluorophores to be targeted to the cytoplasm or nucleus[21]. It is therefore particularly suitable for studies using purified proteins labeled with organic fluorophores or requiring compartment-specific measurements.

Here, the authors describe a protocol covering protein sample requirements, cell culture and seeding, capillary loading and alignment, cytoplasmic or nuclear microinjection, fluorescence imaging, time-resolved single-molecule data acquisition, and subsequent smFRET and correlation analysis. Cy3B- and CF660R-labeled prothymosin α (ProTα) microinjected into adherent HeLa cells is used as a representative system[21], but the overall workflow can be adapted to other proteins, dye pairs, adherent cell types, and intracellular compartments.

Protocol

All the materials used in this study are listed in the **Table of Materials**. No ethical approval was required for this study.

1. Fluorescently labeled protein: quality control and storage

1. Quality control
    1. Use a purified protein of interest that has been site-specifically labeled with a compatible donor-acceptor pair of fluorophores and validated by *in vitro* single-molecule FRET measurements[24,36].
    2. Select dyes with high brightness, photostability, and suitable spectral separation[31].
    3. Verify the purity and expected mass of the doubly labeled protein before injection by reversed-phase high-performance liquid chromatography (RP-HPLC) and electrospray ionization mass spectrometry (ESI-MS)[21].

Copyright © 2026, Journal of Visualized Experiments
Creative Commons Attribution-NonCommercial-NoDerivs 3.0 Unported License

DOI 10.3791/74404

4. Ensure that the sample contains a high proportion of donor-acceptor-labeled protein, minimal donor-only and acceptor-only populations, and negligible free dye.

   NOTE: Dyes excited in the green and red spectral regions are preferred for measurements in living eukaryotic cells because blue excitation produces stronger cellular autofluorescence[21,37]. For the representative measurements described here, prothymosin α (ProTα), an intrinsically disordered protein comprising 110 amino acids, was used. ProTα was labeled at residues 56 and 110 with Cy3B as the donor dye and CF660R as the acceptor dye. High labeling quality is particularly important for intracellular measurements because the available acquisition time and the number of fluorescent molecules are limited. The target concentration for confocal single-molecule detection is approximately 20–100 pM[21], corresponding to roughly 20–100 fluorescent molecules in a HeLa-cell cytoplasmic volume of approximately 1.6 pL[38]. Large donor-only or acceptor-only populations, therefore, reduce the number of informative FRET events and complicate the interpretation of intracellular FRET efficiency distributions.

2. Protein storage

   1. Maintain a concentrated protein stock for microinjection at a concentration at least 100-fold higher than the working concentration used for *in vitro* single-molecule measurements. Divide the labeled protein into small aliquots to avoid repeated freeze-thaw cycles, flash-freeze with liquid nitrogen, and store the aliquots at −80 °C.

      NOTE: The higher concentration required for microinjection compensates for the small injected volume and the subsequent dilution of the protein within the cell. For the representative measurements, ProTα aliquots intended for *in vitro* experiments were prepared at 1–5 nM, which were then diluted ~100-fold for the measurements, whereas concentrated aliquots intended for intracellular experiments were prepared at 100–500 nM. The storage buffer was modified Hanks' balanced salt solution (HBSS) without Ca^{2+} or Mg^{2+}, containing 0.3 mM Na_2HPO_4, 0.4 mM KH_2PO_4, 5.3 mM KCl, 138 mM NaCl, 4.2 mM $NaHCO_3$, and 5.6 mM glucose, adjusted to pH 7.2 and supplemented with 0.01% (v/v) Tween 20[21].

2. Cell culture and seeding before microinjection

1. Cell maintenance

   1. Maintain the selected cell type under its recommended culture conditions. For the representative measurements, maintain the cells in T25 culture flasks with filter caps at 37 °C in a humidified atmosphere containing 5% CO_2.

   2. Use FluoroBrite DMEM supplemented with GlutaMAX, 10% fetal bovine serum, 100 units/ml penicillin, and 0.1 mg/ml streptomycin.

      NOTE: Conventional DMEM containing phenol red produces excessive fluorescence background and is not recommended for intracellular single-molecule measurements. FluoroBrite DMEM is preferred for maintaining a low fluorescence background. For cell lines that cannot be maintained robustly in FluoroBrite DMEM over extended periods, use high-glucose DMEM containing pyruvate but without phenol red. This medium produces a slightly higher but still acceptable fluorescence background.

   3. Passage the cells when they reach 70–80% confluence. Perform all cell-culture procedures using aseptic technique in a biosafety cabinet.

   4. Aspirate the culture medium and wash the cells once with 5 mL of phosphate-buffered saline. Remove the phosphate-buffered saline and add 0.6 mL of 0.05% phenol-red-free trypsin prewarmed to 37 °C.

   5. Incubate the cells at 37 °C in a humidified atmosphere containing 5% CO_2 for 2–5 min until the cells detach.

   6. Add 5 mL of prewarmed culture medium and gently resuspend the detached cells. Transfer 1–2 mL of the cell suspension into a new T25 flask containing 5 mL of prewarmed culture medium. Gently tilt the flask to distribute the cells evenly and return it to the incubator.

2. Cell seeding in imaging dishes: One day before microinjection, select a T25 flask containing healthy cells at 70–80% confluence. Aspirate the culture medium and detach the cells as described in steps 2.1.4–2.1.5.

   1. Add 2 mL of prewarmed culture medium to each 35-mm glass-bottom imaging dish. Prepare 2–6 dishes for one measurement day.

   2. Resuspend the detached cells in 5 mL of prewarmed culture medium. Transfer 0.5 mL of the cell suspension to each prepared imaging dish and gently move the dish to distribute the cells evenly across the glass surface.

   3. Incubate the dishes overnight at 37 °C in a humidified atmosphere containing 5% CO_2. At the time of microinjection, aim for 10–30% confluence, with

Copyright © 2026, Journal of Visualized Experiments
Creative Commons Attribution-NonCommercial-NoDerivs 3.0 Unported License

DOI 10.3791/74404

individual cells spatially separated and accessible to the microinjection capillary.

NOTE: Uncoated glass-bottom dishes are preferred to minimize fluorescence background. This approach is most suitable for cell lines that adhere efficiently to untreated glass. If surface coating is required for cell adhesion, measure the fluorescence background of the coated dish under the same excitation and detection conditions before performing the experiment and confirm that it is sufficiently low for single-molecule measurements.

3. Microinjection system setup on the day of measurement

1. Capillary preparation and loading
    1. Remove the protective cap from the microinjection capillary by strictly following the manufacturer's instructions.
    2. Hold the capillary vertically with the fine tip pointing downward, slowly loosen the protective cap, and allow the cap to fall under gravity without contacting the fine capillary tip. Carefully place the capillary in a holder with the fine tip pointing upward.
    3. Prepare 2–3 µL of injection solution containing 50 nM fluorescently labeled protein in modified HBSS without Ca^{2+} or Mg^{2+}, supplemented with 0.005% (v/v) Tween 20.

        NOTE: For a new protein, use 50 nM as the starting injection concentration and optimize it by adjusting the injection pulse duration. Under the representative conditions, a 20–50 nM injection solution yields estimated intracellular concentrations of approximately 50–500 pM, corresponding to a 40–1,000-fold dilution[21]. Decrease the concentration if individual bursts cannot be resolved, or increase it if too few bursts are obtained. The optimal concentration depends on fluorophore brightness, protein adsorption, diffusion, and the selected cell type.
    4. Use a 100-mm-long microloader tip to transfer the injection solution into the capillary. Insert the microloader through the wide end of the capillary and dispense the solution as close as possible to the narrow end.

        NOTE: Tween 20 is included at 0.005% (v/v) to reduce protein adsorption to surfaces during sample preparation and delivery[21]. Upon injection, it is further diluted within the cell to a concentration that is one to three orders of magnitude below its critical micelle concentration. Under the conditions described here, approximately 90% of injected HeLa cells retain normal morphology and remain suitable for measurement. However, compatibility should be assessed for each cell type and experimental readout.
    5. Inspect the loaded capillary for internal air bubbles that separate the injection solution into two or more liquid segments. If an internal bubble is present, gently tap the wide end of the capillary until the solution forms a continuous, uninterrupted liquid column.

        NOTE: Internal air bubbles must be removed because they are compressed when pressure is applied, reducing pressure transmission to the solution at the capillary tip and preventing reliable injection. In contrast, a small air-filled space between the continuous liquid column and the extremely fine capillary tip is acceptable before priming. The injection pulses described expel this terminal air and drive the solution to the tip.
    6. Mount the capillary onto the microinjector and secure it finger-tight. Keep the capillary holder at its highest vertical position to provide sufficient space for placing the imaging dish on the microscope stage.

        NOTE: The pressure-driven microinjection apparatus used here consists of a joystick-controlled three-axis micromanipulator carrying a capillary holder connected to a pressure controller. The controller allows independent adjustment of the injection pressure, pulse duration, and compensation pressure. The capillary holder and pressure controller used for the representative experiments were custom-built. Equivalent commercial systems can also be used.
    7. Apply one or more brief injection pulses sufficient to expel the remaining air and bring the injection solution to the fine tip. For the representative system, use a pressure of 1 bar, a pulse duration of 80 ms, and apply two pulses to expel.
    8. Apply a low continuous compensation pressure sufficient to prevent the imaging medium from entering the capillary. For the representative system, use 0.05 bar. Keep the prepared capillary mounted while preparing the cells for microinjection.
2. Cells: imaging-buffer exchange and microscope placement
    1. Remove one imaging dish from the incubator. Visually inspect the cells and confirm suitable confluence, normal morphology, and firm attachment to the glass surface. Aspirate the culture medium and wash the cells once with 2 mL of modified HBSS containing Ca^{2+} and Mg^{2+} but no sodium bicarbonate.

Copyright © 2026, Journal of Visualized Experiments
Creative Commons Attribution-NonCommercial-NoDerivs 3.0 Unported License

DOI 10.3791/74404

2. Prepare this buffer with 1.3 mM $CaCl_2$, 0.5 mM $MgCl_2$, 0.4 mM $MgSO_4$, 0.3 mM Na_2HPO_4, 0.4 mM KH_2PO_4, 5.3 mM KCl, 138 mM NaCl, and 5.6 mM glucose, adjusted to pH 7.2.

   NOTE: Use bicarbonate-free imaging buffer when performing microinjection, imaging, and data acquisition at room temperature under ambient air. If the complete experiment is performed at 37 °C in an atmosphere containing 5% CO_2, use an imaging medium containing sodium bicarbonate.

3. Aspirate the washing buffer and add 2 mL of fresh modified HBSS containing Ca^{2+} and Mg^{2+} but no sodium bicarbonate.

   NOTE: As a conservative practical guideline, complete microinjection, imaging, and data acquisition within 1 h after exchanging the medium. This minimizes time-dependent changes in cell physiology during incubation in HBSS at room temperature under ambient air. Cell morphology and membrane integrity have been shown to remain preserved for up to 1.5 h under optimized microinjection conditions[37]. Prepare and measure only one imaging dish at a time.

4. Apply a drop of immersion water on top of the 60x water-immersion objective and place the imaging dish on the microscope stage. Position the central area of the glass-bottom surface above the objective and focus on the cells using bright-field illumination.

   NOTE: Water immersion is recommended for intracellular single-molecule measurements because it combines high numerical aperture with reduced refractive-index mismatch in aqueous samples. Dry or oil-immersion objectives may also be used for microinjection. Their suitability for the subsequent single-molecule measurements, however, is low because of the low collection efficiency and low working distance, respectively.

3. Capillary alignment with the observation field

   1. Slowly lower the capillary until its tip just contacts the surface of the imaging medium. Set the micromanipulator joystick to the coarsest movement setting (mode 1 on the representative instrument). Move the capillary laterally in the x-y plane until it is positioned approximately above the center of the objective.

      NOTE: The numbered movement modes are speed and movement-range settings specific to the micromanipulator used here. Mode 1 provides coarse movement, and increasing mode numbers provide progressively finer positioning, with mode 5 used for final positioning and microinjection. When using a different micromanipulator, select the corresponding coarse, intermediate, and fine movement settings.

   2. Observe the cells through the eyepiece under Köhler transmitted-light illumination while maintaining focus on the cell plane.

   3. Move the capillary broadly across the area above the objective until its shadow becomes visible. Stop moving the capillary as soon as the shadow appears, and switch the joystick to the intermediate movement setting (mode 2).

   4. Move the capillary slowly in the x–y plane along the outline of its shadow until the narrow end becomes visible. Using an eyepiece containing a crosshair reticle, position the end of the shadow at the center of the field of view. Switch the joystick to fine movement setting (mode 3 or 4) to restrict further lateral movement.

   5. Slowly lower the capillary vertically along the z-axis until the fine tip comes into focus. Make small adjustments in the x–y plane as necessary to keep the tip centered. Once the final position is reached, switch the joystick to the finest movement setting (mode 5).

   6. Confirm that the cells and the fine capillary tip are sharply focused simultaneously. The wider portion of the capillary may remain slightly out of focus.

4. Cell microinjection, fluorescence imaging, and data acquisition

1. Cell microinjection

   1. Using movement mode 5, raise the capillary slightly along the z-axis to allow the cells to pass freely underneath it without contacting the capillary tip.

   2. Switch to differential interference contrast (DIC) imaging to improve visualization of the cell boundary, cytoplasm, nucleus, and capillary tip. Move the microscope stage to select a healthy, spatially isolated cell and position it at the center of the field of view.

   3. Move the fine end of the capillary toward the selected cell and position the tip over the desired injection site within the cytoplasm. Slowly lower the capillary until a slight local indentation of the plasma membrane becomes visible, indicating contact with the cell surface.

   4. Without lowering the capillary further into the cell, trigger the injection pulse to deliver the labeled protein into the cytoplasm. Withdraw and raise the capillary immediately after the injection.

Copyright © 2026, Journal of Visualized Experiments
Creative Commons Attribution-NonCommercial-NoDerivs 3.0 Unported License

DOI 10.3791/74404

NOTE: For cytoplasmic injection, the cell membrane is not penetrated by the capillary tip, only by the jet of sample solution, and the membrane reseals directly after the injection pulse. A subtle and rapid displacement or deformation of the cell is typically visible following successful injection. Excessive or prolonged deformation may indicate overinjection or cell damage.

5. Optimize the injection pressure and pulse duration according to the protein concentration, protein adsorption to the capillary surface, sample viscosity, capillary geometry, and cell type and size.

   NOTE: For the representative measurements, 50 nM Cy3B- and CF660R-labeled ProTα were injected into HeLa cells using an injection pressure of 1 bar and a pulse duration of 80 ms.

6. For nuclear injection, lower the capillary further until the tip gently penetrates the plasma membrane and nuclear envelope. Trigger the injection pulse once the tip is positioned within the nucleus. Withdraw and raise the capillary immediately after the injection.

   NOTE: A brief, subtle expansion of the nucleus may be observed following successful nuclear injection. Avoid excessive nuclear swelling, which may indicate over-injection or cell damage. Align the glass surface of the culture dish as closely as possible with the plane of x–y stage motion. Because small differences in surface height or alignment may change the clearance during lateral movement, raise the capillary sufficiently before moving the stage to allow cells to pass freely underneath it and prevent the tip from contacting the glass. Otherwise, the capillary may detach cells from the dish or get damaged.

2. Cell imaging and measurement-site selection

   1. Perform fluorescence imaging and single-molecule measurements on an inverted confocal microscope equipped with differential interference contrast imaging and a 60x water-immersion objective with a numerical aperture of 1.20.

   2. Collect the fluorescence through the objective and a 100-µm-diameter confocal pinhole, and spectrally separate it into donor and acceptor emission channels. The radial $1/e^2$ radius of the confocal detection volume was $w_{xy} \approx 0.3$ µm.

   3. Detect the fluorescence in both channels simultaneously using single-photon-counting detectors, and route the detector outputs and laser-synchronization signals to a time-correlated single-photon-counting module for time-tagged photon recording.

      NOTE: The representative ProTα measurements were performed at room temperature (22 °C).

   4. Position the injected cell at the center of the field of view. Turn off the bright-field illumination, switch to fluorescence-acquisition mode, and activate the required excitation lasers and detector channels.

   5. Select the excitation mode according to the required fluorescence information. For alternating-laser excitation (ALEX)[25], alternate donor and acceptor excitation and record fluorescence simultaneously in the donor and acceptor detection channels during each excitation period.

   6. Use the donor- and acceptor-channel photons detected during donor excitation to determine the FRET efficiency. Use acceptor-channel photons detected during direct acceptor excitation to verify the presence of an active acceptor and determine the donor-acceptor stoichiometry ratio[25,39].

   7. Use pulsed interleaved excitation (PIE) when fluorescence-lifetime information is also required[26].

   8. For PIE, interleave donor and acceptor excitation pulses and assign each detected photon to its corresponding excitation pulse based on the photon arrival time relative to the laser-synchronization signal.

   9. Alternatively, use single-color continuous-wave excitation when neither direct acceptor excitation nor fluorescence lifetime information is required, or single-color pulsed excitation when fluorescence lifetime or nsFCS information is required without direct acceptor excitation.

      NOTE: Both ALEX and PIE enable donor-acceptor stoichiometry ratio analysis. In the configuration described here, ALEX is preferred for routine intracellular burst measurements because the high peak intensities associated with pulsed excitation may promote transitions to long-lived dark states and increase the rate of photobleaching[40]. For the representative ALEX measurements, set the 515 nm and 642 nm excitation powers to 50 µW and 20 µW, respectively, measured at the back aperture of the objective. Alternate the lasers at 10 kHz with duty cycles of 70% and 30% for the 515 nm and 642 nm lasers, respectively.

   10. Acquire a rapid-scan image of the injected cell with a short dwell time per pixel to minimize photobleaching. For the representative measurements, scan an area of

Copyright © 2026, Journal of Visualized Experiments
Creative Commons Attribution-NonCommercial-NoDerivs 3.0 Unported License

DOI 10.3791/74404

80 µm x 80 µm using 128 x 128 pixels and a pixel dwell time of ~0.7 ms.

11. Confirm that the injected cell retains normal morphology and exhibits a fluorescence signal above the background observed in neighboring non-injected cells, which serve as a reference.

NOTE: Depending on the molecule's ability to enter the nucleus and its interactions with intracellular components, fluorescence may be observed predominantly in the cytoplasm, in the nucleus, or throughout the cell. Select a confocal measurement position within the intracellular region of interest, such as the cytoplasm or nucleus.

3. Intracellular single-molecule data acquisition

1. Position the confocal observation volume at the selected intracellular location and start the time-tagged photon acquisition. For the representative measurements, record each injected cell for 3 min.

NOTE: Under optimized conditions, approximately 90% of injected HeLa cells remain viable. When injection and measurement are performed sequentially, approximately 10 cells can be injected and measured per hour. Approximately 200–800 fluorescence bursts are typically obtained from each cell during a 3-min measurement, although burst numbers vary because of differences in injection efficiency and photobleaching[21]. Intracellular concentrations were estimated by comparison with *in vitro* burst frequencies to be approximately 50–500 pM[21].

5. Single-molecule fluorescence data processing and analysis

1. FRET-efficiency analysis

1. Analyze the time-tagged photon data using Fretica, a custom Wolfram Mathematica add-on package for single-molecule fluorescence analysis available at https://github.com/SchulerLab/Fretica.

2. Follow the documented instructions to set up the detection route and micro-time channel assignment. Set the correction factors that correct for cross-talk, differences in detection efficiency and quantum yield, and direct excitation of the laser.

NOTE: Determine the correction factors from separate calibration measurements. Determine donor crosstalk from a donor-only sample and direct acceptor excitation from an acceptor-only sample. Determine the γ factor, which accounts for differences in fluorescence quantum yield and detection efficiency, using donor-acceptor-labeled reference samples spanning a range of FRET efficiencies. Repeat the calibration when the dye pair or detection configuration is changed. Detailed procedures are described by Holmstrom et al.[39].

3. Divide the photon time-trace into segments. Determine the fluorescence background and choose a burst-selection threshold separately for each segment. Use shorter segments at the beginning, when photobleaching is more rapid, and longer segments later in the measurement.

4. For the representative 180-s measurements, use the intervals 0–5, 5–15, 15–40, 40–80, 80–120, 120–150, and 150–180 s. Adjust these intervals according to the photobleaching behavior of the sample.

NOTE: Analyze the segments separately because background count rates change during intracellular photobleaching. Applying a single background estimate to the entire trace may bias the fluorescence corrections and broaden or shift the resulting FRET efficiency and stoichiometry distributions.

5. Identify fluorescence bursts using dual-channel burst search with a maximal inter-photon time of 40 µs[41]. For the representative analysis, retain only bursts with a corrected photon number of at least 30 to obtain sufficient photon statistics for reliable FRET-efficiency estimation.

6. Exclude exceptionally bright bursts that are clear outliers in the burst photon-count distribution, as these may arise from molecular aggregates, surface-associated molecules, or other artifacts.

7. Combine bursts from time segments with sufficiently stable fluorescence signals and calculate corrected FRET efficiency *E* and stoichiometry *S*:

$$E = \frac{n_{DA}}{n_{DD}+n_{DA}} \quad (1)$$

$$S = \frac{n_{DD}+n_{DA}}{n_{DD}+n_{DA}+n_{AA}} \quad (2)$$

where n_{DD} and n_{DA} are the corrected donor- and acceptor-channel photon numbers detected following donor excitation, respectively, and n_{AA} is the corrected acceptor-channel photon number detected following acceptor excitation. For a detailed description of the corrections for donor crosstalk and direct acceptor excitation, refer to Schuler et al.[24].

8. Fit the FRET-efficiency histogram using peak functions appropriate for the sample. With dual-channel burst identification, donor-only bursts have already been

Copyright © 2026, Journal of Visualized Experiments
Creative Commons Attribution-NonCommercial-NoDerivs 3.0 Unported License

DOI 10.3791/74404

excluded. Obtain the mean FRET efficiency from the fitted donor-acceptor distribution[39].

NOTE: For the representative ProTα data, a single Gaussian is sufficient to describe this population. Inspect the FRET efficiency histogram across temporal segments and the corresponding diffusion times. Stable histograms and the absence of new single-color or faster-diffusing populations support protein integrity over the measurement period. However, fluorescence measurements alone cannot exclude a proteolytic fragment that retains both dyes.

2. FCS analysis

    1. Calculate the donor-acceptor fluorescence cross-correlation curve from the time-tagged photon data.

$$G_{ij}(\tau) = \frac{\langle \delta I_i(t) \delta I_j(t+\tau) \rangle}{\langle I_i(t) \rangle \langle I_j(t) \rangle} \qquad (3)$$

    where $\delta I_i(t) = I_i(t) - \langle I_i(t) \rangle$. When $i = j$, this expression describes an autocorrelation; when $i \neq j$, it describes a cross-correlation between the donor and acceptor channels[27].

    2. For the representative analysis, omit the first 80 s, during which photobleaching causes a pronounced decrease in fluorescence intensity that introduces an additional component into the correlation function.

    3. For each measurement, omit the initial interval until the count rate has stabilized and no systematic intensity decay is evident. Calculate the correlation curve over lag times from 10^{-5} to 1 s using a logarithmic binning of 0.05 decades.

    4. Fit the correlation curve, for example, with the common diffusion model that assumes a 3D Gaussian molecular detection function:

$$G(\tau) = G(0)\left(1 + \frac{\tau}{\tau_D}\right)^{-1}\left(1 + \frac{\tau}{s^2\tau_D}\right)^{-\frac{1}{2}} + G_\infty \qquad (4)$$

    where τ_D is the characteristic diffusion time, s is the axial-to-lateral dimension ratio of the confocal volume, which was independently measured to be 6 in the representative instrument, and G_∞ is the baseline offset. If needed, include a term for triplet-blinking.

    5. Obtain the characteristic diffusion time from the fitted curve and inspect the fit residuals for systematic deviations, which may be caused by aggregates, photobleaching, focus drift, or other factors[21,27].

3. nsFCS analysis

    1. Calculate the donor-donor and acceptor-acceptor autocorrelation functions and the donor-acceptor cross-correlation function from the time-tagged photon trace using the correlation definition given in 5.2.1, with linearly spaced lag-time intervals extending up to a few microseconds[28,29].

    NOTE: Because nsFCS requires sufficient photon statistics, average the correlation functions obtained from multiple cells measured under the same conditions. As a practical starting point, acquire approximately 3 minutes per cell from 30–50 cells.

    2. Fit all three obtained correlation functions globally with a model accounting for antibunching, triplet-state blinking, and chain dynamics. Interdye-distance fluctuations produce positive correlation components in the donor-donor and acceptor-acceptor autocorrelation functions and an anticorrelated component in the donor-acceptor cross-correlation function.

    3. Determine the chain-reconfiguration time by using it as a shared parameter across all three correlation functions[28,29].

Results

The protocol described here was applied to Cy3B- and CF660R-labeled prothymosin α (ProTα)[21,30,36], an intrinsically disordered protein, in adherent HeLa cells. A 50 nM solution of FRET-labeled ProTα was loaded into the microinjection capillary with 0.5 µm inner diameter and delivered using an injection pressure of 1 bar and a pulse duration of 80 ms. **Figure 1A** summarizes the workflow from preparation of the injection solution and capillary loading to cell injection and single-molecule fluorescence data acquisition. Following cytoplasmic injection, fluorescence lifetime imaging confirmed delivery of the labeled protein and guided selection of an intracellular measurement position, while DIC imaging was used to monitor cell morphology. In **Figure 1B**, lifetime maps are overlaid on selected cytoplasmic regions of the DIC image, showing longer fluorescence lifetimes from labeled ProTα in the injected cell (green) and shorter-lived cellular autofluorescence in the neighboring non-injected cell (blue). In this example, labeled ProTα is predominantly located in the cytoplasm.

At a selected confocal position in the cytoplasm, the fluorescence intensity initially decreased owing to photobleaching of the intracellular fluorophores[21] (**Figure 1C**). The trace displayed with 1 s binning shows this characteristic decay, whereas displaying a selected interval with 1 ms binning resolves discrete donor and acceptor fluorescence bursts originating from individual molecules diffusing through the confocal volume. Individual bursts are resolvable from the beginning of the acquisition, while temporal segmentation accounts for changes in background during photobleaching. A successful acquisition therefore provides

Copyright © 2026, Journal of Visualized Experiments
Creative Commons Attribution-NonCommercial-NoDerivs 3.0 Unported License

DOI 10.3791/74404

clearly distinguishable individual bursts and sufficient burst counts for quantitative analysis.

To account for changes in the fluorescence background during photobleaching, the 180 s photon trace was divided into consecutive segments (**Figure 2A**). Shorter segments were used at the beginning of the measurement, when the fluorescence intensity and burst frequency were high, whereas longer segments were used at later times to obtain sufficient photon statistics[21]. Within each segment, the background count rate and burst-search threshold were determined independently. The bursts identified in each segment were corrected using the corresponding local background and used to construct segment-specific FRET efficiency histograms. Despite the changes in fluorescence intensity and burst frequency over time, the histograms consistently contained a donor-only population near E = 0 and a FRET population near E = 0.35 (**Figure 2B**). The accepted bursts from all segments were then pooled to generate the combined FRET efficiency histograms (**Figure 2C**). In the FRET efficiency-stoichiometry (E-S) contour plot shown in the inset of **Figure 2C**, donor-only molecules are located near S = 1, acceptor-only molecules near S = 0 (there are negligible acceptor-only molecules in this sample), and donor-acceptor-labeled ProTα form a distinct population near S = 0.5. For **Figure 2D**, dual-channel burst identification was used to largely exclude the donor-only population, yielding a single FRET population with a mean FRET efficiency of 0.35 (**Figure 2D**).

Alternatively, donor-only bursts in ALEX data can be excluded by applying a stoichiometry filter, such as 0.2 < S < 0.8. Individual molecules can pass repeatedly through the confocal volume, so the histograms count detection events rather than distinct molecules. Repeated detection improves burst statistics from the limited intracellular pool of molecules[21]. Measurements from 5–10 independent cells provide a practical starting point for estimating cell variability in the mean FRET efficiency. Previous ProTα measurements using 8 cells yielded a cell-to-cell standard deviation of 0.02[21]. These representative results show that segment-specific background correction accommodates the changing fluorescence background during photobleaching, while dual-channel burst identification or stoichiometry-based selection isolates the donor-acceptor-labeled population for reliable determination of the intracellular FRET efficiency.

The same time-tagged photon data used for the burst analysis in **Figure 2A–D** were also analyzed by donor-acceptor fluorescence cross-correlation spectroscopy to determine translational diffusion. Compared with the *in vitro* correlation curve, the representative cytosolic curve was shifted toward longer lag times, indicating slower diffusion of ProTα in the intracellular environment (**Figure 2E**). Fitting the curves with a one-component three-dimensional diffusion model yielded diffusion times, τ_D, of 0.43 ms *in vitro* and 1.12 ms in the cytosol. Thus, the representative measurement demonstrates that the same photon data can be used to quantify both the conformational properties and translational diffusion of intracellular ProTα.

Nanosecond fluorescence correlation spectroscopy (nsFCS) can additionally be applied to time-tagged photon data to quantify rapid intramolecular dynamics[21,28,29,37]. **Figure 2F** illustrates representative nsFCS correlation functions obtained for donor-acceptor-labeled ProTα in the cytosol of osmotically stressed HeLa cells from in-cell measurements[37]. As the disordered ProTα chain reconfigures among conformations with different interdye distances, the resulting changes in FRET efficiency produce anticorrelated fluctuations in donor and acceptor fluorescence. A decrease in interdye distance increases acceptor fluorescence and decreases donor fluorescence, whereas an increase in distance has the opposite effect. These fluctuations, therefore, produce positive relaxation components in the donor-donor and acceptor-acceptor autocorrelation functions and an anticorrelated component in the donor-acceptor cross-correlation function. Global analysis of the three correlation functions separates the contribution of chain dynamics from antibunching and triplet-state blinking and determines the timescale of chain reconfiguration. The observed correlation pattern demonstrates rapid submicrosecond chain reconfiguration of ProTα inside cells.

Copyright © 2026, Journal of Visualized Experiments
Creative Commons Attribution-NonCommercial-NoDerivs 3.0 Unported License

DOI 10.3791/74404

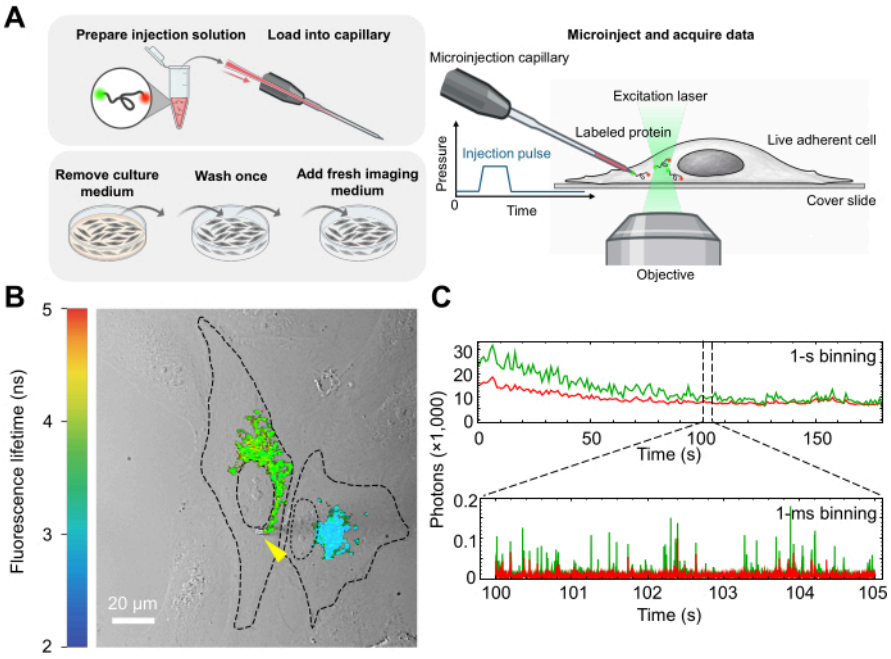

Figure 1: Workflow and representative fluorescence measurements following microinjection of labeled protein into living cells. (**A**) Schematic overview of the experimental workflow. The fluorescently labeled protein is diluted into the injection buffer, loaded into a microinjection capillary, and delivered into an adherent cell by a pressure pulse. After exchanging the culture medium for imaging medium, the injected cell is imaged, and fluorescence is recorded from a selected intracellular confocal volume. The schematic was partially created using BioRender. (**B**) Representative fluorescence lifetime imaging microscopy (FLIM) image overlaid on selected cytoplasmic regions of a differential interference contrast (DIC) image. The longer fluorescence lifetimes in the injected HeLa cell (green) arise from Cy3B- and CF660R-labeled ProTα, whereas the neighboring non-injected cell exhibits shorter-lived cellular autofluorescence (blue). The yellow arrow indicates the position of the capillary tip. Scale bar, 20 µm. (**C**) Donor- and acceptor-channel photon-count traces acquired at a fixed cytoplasmic position in an injected cell. At 1-s binning, the gradual decrease in fluorescence intensity reflects photobleaching. Enlargement of a selected interval using 1-ms binning resolves fluorescence bursts generated by individual molecules passing through the confocal observation volume. Donor and acceptor photon counts are shown in green and red, respectively.
Please click here to view a larger version of this figure.

Copyright © 2026, Journal of Visualized Experiments
Creative Commons Attribution-NonCommercial-NoDerivs 3.0 Unported License

DOI 10.3791/74404

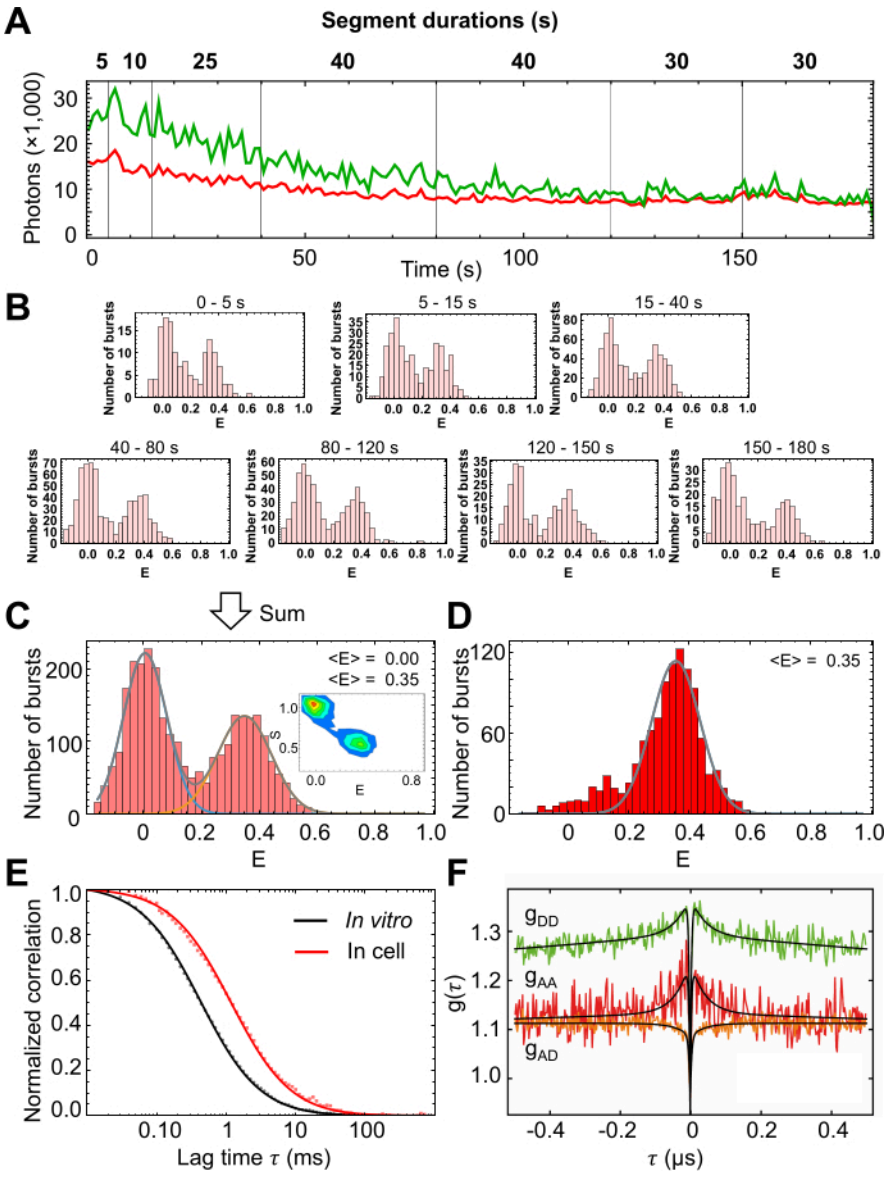

Figure 2: Analysis of the conformation, translational diffusion, and chain dynamics of microinjected ProTα. (**A**) Donor- and acceptor-channel photon-count traces recorded for 180 s at a fixed cytoplasmic position in a ProTα-injected HeLa cell. The trace was divided into intervals of different durations so that the changing fluorescence background caused by photobleaching could be determined separately for each interval. (**B**) Background-corrected FRET-efficiency histograms calculated independently for the time intervals indicated in (**A**). (**C**) Combined FRET-efficiency histogram obtained by pooling the bursts from the individual time intervals. The inset shows the corresponding two-dimensional FRET efficiency-stoichiometry (E-S) contour plot, revealing a donor-only population near S = 1 and a donor-acceptor-labeled FRET population near S = 0.5. (**D**) FRET efficiency histogram obtained using dual-channel burst identification to exclude donor-only bursts. The gray line represents a Gaussian fit to the remaining FRET population. The histogram contains 2,178 bursts. (**E**) Representative donor-acceptor fluorescence cross-correlation curves for ProTα *in vitro* (black) and in the cytosol of the same cell analyzed in panels **A–D** (red). Data points represent the measured correlation functions. Solid lines indicate fits to a one-component three-dimensional diffusion model, yielding diffusion times of 0.43 ms *in vitro* and 1.12 ms in the cytosol. (**F**) nsFCS correlation functions of donor-acceptor-labeled ProTα in the cytosol of osmotically stressed HeLa cells, obtained from 33 in-cell measurements. Donor-donor and acceptor-acceptor autocorrelation functions and the donor-acceptor cross-correlation function are shown together with the global fits. The positive autocorrelation and negative cross-correlation components originate from rapid fluctuations in the interdye distance during ProTα chain reconfiguration. Adapted from König et al. with copyright permission[37]. Please click here to view a larger version of this figure.

Discussion

Here, the authors presented a protocol for introducing dye-labeled proteins into individual living eukaryotic cells by microinjection, followed by fluorescence imaging and confocal single-molecule fluorescence spectroscopy. Successful implementation requires careful coordination of protein labeling quality, capillary loading, cell handling, injection parameters, fluorescence imaging, and photon acquisition. In particular, the injection solution must

Copyright © 2026, Journal of Visualized Experiments
Creative Commons Attribution-NonCommercial-NoDerivs 3.0 Unported License

contain a high proportion of donor-acceptor-labeled protein, the capillary must provide stable and uninterrupted flow, and the injection pressure and pulse duration must be optimized to achieve sufficient delivery while maintaining normal cell morphology. Low-autofluorescence imaging conditions and background determination are also essential for resolving single-molecule fluorescence bursts during intracellular photobleaching[21,23,40].

As with other in-cell single-molecule measurements, photobleaching limits the observation time and number of detectable bursts[32,40]. Microinjection facilitates optimization by allowing a broad choice of fluorophores, purification of a well-defined population of doubly labeled molecules, and flexible yet reproducible adjustment of the in-cell concentration. Practical limitations of microinjection include its relatively low throughput and the need for specialized equipment and operator training. Capillary blockage and cell damage can generally be minimized by testing capillary flow before injection and optimizing the injection pressure and pulse duration while monitoring cell morphology.

Using the dye-labeled IDP ProTα in HeLa cells as a representative system, this workflow enables measurements of intracellular localization, conformational distributions, translational diffusion, and rapid chain dynamics through fluorescence imaging, smFRET, FCS, and nsFCS[6,27,29]. The protocol can be adapted to other proteins, dye pairs, adherent cell types, and cytoplasmic or nuclear measurements. Future applications that are expected to benefit from microinjection-based in-cell smFRET include investigating protein folding, intrinsically disordered proteins, molecular recognition, protein-protein interactions, biomolecular phase separation, and compartment-dependent conformational behavior[3,21,30].

Disclosures

All authors have read and approved the manuscript. They declare no conflict of interest.

Acknowledgments

This work was supported by Swiss National Science Foundation (SNSF) grants 10006187, CRSII5_205922, and 200021_219629, and Forschungskredit of the University of Zurich FK-24-055.

References

1. Henzler-Wildman K, Kern D. Dynamic personalities of proteins. Nature. 2007;450(7172):964–972.
2. Frauenfelder H, Sligar SG, Wolynes PG. The energy landscapes and motions of proteins. Science. 1991;254(5038):1598–1603.
3. Boehr DD, Nussinov R, Wright PE. The role of dynamic conformational ensembles in biomolecular recognition. Nat Chem Biol. 2009;5(11):789–796.
4. Schuler B, Lipman EA, Eaton WA. Probing the free-energy surface for protein folding with single-molecule fluorescence spectroscopy. Nature. 2002;419(6908):743–747.
5. Schuler B, Hofmann H. Single-molecule spectroscopy of protein folding dynamics—expanding scope and timescales. Curr Opin Struct Biol. 2013;23(1):36–47.
6. Schuler B, Soranno A, Hofmann H, Nettels D. Single-molecule FRET spectroscopy and the polymer physics of unfolded and intrinsically disordered proteins. Annu Rev Biophys. 2016;45:207–231.
7. Zhou HX, Rivas G, Minton AP. Macromolecular crowding and confinement: biochemical, biophysical, and potential physiological consequences. Annu Rev Biophys. 2008;37:375–397.
8. Ebbinghaus S, Dhar A, McDonald JD, Gruebele M. Protein folding stability and dynamics imaged in a living cell. Nat Methods. 2010;7(4):319–323.
9. Guo M, Xu Y, Gruebele M. Temperature dependence of protein folding kinetics in living cells. Proc Natl Acad Sci U S A. 2012;109(44):17863–17867.
10. Wang Y, Sukenik S, Davis CM, Gruebele M. Cell volume controls protein stability and compactness of the unfolded state. J Phys Chem B. 2018;122(49):11762–11770.
11. Sukenik S, Salam M, Wang Y, Gruebele M. In-cell titration of small solutes controls protein stability and aggregation. J Am Chem Soc. 2018;140(33):10497–10503.
12. Chowdhury A et al. Driving forces of the complex formation between highly charged disordered proteins. Proc Natl Acad Sci U S A. 2023;120(41):e2304036120.
13. Uversky VN. What does it mean to be natively unfolded? Eur J Biochem. 2002;269(1):2–12.
14. Müller-Späth S et al. Charge interactions can dominate the dimensions of intrinsically disordered proteins. Proc Natl Acad Sci U S A. 2010;107(33):14609–14614.
15. Soranno A et al. Single-molecule spectroscopy reveals polymer effects of disordered proteins in crowded environments. Proc Natl Acad Sci U S A. 2014;111(13):4874–4879.
16. Phillip Y, Kiss V, Schreiber G. Protein-binding dynamics imaged in a living cell. Proc Natl Acad Sci U S A. 2012;109(5):1461–1466.
17. Berezin MY, Achilefu S. Fluorescence lifetime measurements and biological imaging. Chem Rev. 2010;110(5):2641–2684.
18. Smith AE, Zhang Z, Pielak GJ, Li C. NMR studies of protein folding and binding in cells and cell-like environments. Curr Opin Struct Biol. 2015;30:7–16.
19. Luchinat E, Cremonini M, Banci L. Radio signals from live cells: the coming of age of in-cell solution NMR. Chem Rev. 2022;122(10):9267–9306.
20. Young LN, Villa E. Bringing structure to cell biology with cryo-electron tomography. Annu Rev Biophys. 2023;52:573–595.
21. König I et al. Single-molecule spectroscopy of protein conformational dynamics in live eukaryotic cells. Nat Methods. 2015;12(8):773–779.
22. Persson F, Barkefors I, Elf J. Single molecule methods with applications in living cells. Curr Opin Biotechnol. 2013;24(4):737–744.
23. Sisamakis E, Valeri A, Kalinin S, Rothwell PJ, Seidel CAM. Accurate single-molecule FRET studies using multiparameter fluorescence detection. Methods Enzymol. 2010;475:455–514.
24. Schuler B, Müller-Späth S, Soranno A, Nettels D. Application of confocal single-molecule FRET to intrinsically disordered proteins. Methods Mol Biol. 2012;896:21–45.

Copyright © 2026, Journal of Visualized Experiments
Creative Commons Attribution-NonCommercial-NoDerivs 3.0 Unported License

DOI 10.3791/74404

25. Kapanidis AN et al. Alternating-laser excitation of single molecules. Acc Chem Res. 2005;38(7):523–533.
26. Müller BK, Zaychikov E, Bräuchle C, Lamb DC. Pulsed interleaved excitation. Biophys J. 2005;89(5):3508–3522.
27. Mütze J, Ohrt T, Schwille P. Fluorescence correlation spectroscopy *in vivo*. Laser Photonics Rev. 2011;5(1):52–67.
28. Nettels D, Gopich IV, Hoffmann A, Schuler B. Ultrafast dynamics of protein collapse from single-molecule photon statistics. Proc Natl Acad Sci U S A. 2007;104(8):2655–2660.
29. Soranno A et al. Quantifying internal friction in unfolded and intrinsically disordered proteins with single-molecule spectroscopy. Proc Natl Acad Sci U S A. 2012;109(44):17800–17806.
30. Galvanetto N et al. Extreme dynamics in a biomolecular condensate. Nature. 2023;619(7971):876–883.
31. Plochowietz A, Crawford R, Kapanidis AN. Characterization of organic fluorophores for *in vivo* FRET studies based on electroporated molecules. Phys Chem Chem Phys. 2014;16(25):12688–12694.
32. Crawford R et al. Long-lived intracellular single-molecule fluorescence using electroporated molecules. Biophys J. 2013;105(11):2439–2450.
33. Plochowietz A, El-Sagheer AH, Brown T, Kapanidis AN. Stable end-sealed DNA as robust nano-rulers for *in vivo* single-molecule fluorescence. Chem Sci. 2016;7(7):4418–4422.
34. Okamoto K, Hibino K, Sako Y. In-cell single-molecule FRET measurements reveal three conformational state changes in RAF protein. Biochim Biophys Acta Gen Subj. 2020;1864(2):129358.
35. Anandamurugan A et al. Single-molecule FRET and tracking of transfected biomolecules in living cells. Biophys J. 2026;125(12):3025–3033.
36. Zosel F, Holla A, Schuler B. Labeling of proteins for single-molecule fluorescence spectroscopy. Methods Mol Biol. 2022;2376:207–233.
37. König I, Soranno A, Nettels D, Schuler B. Impact of in-cell and in-vitro crowding on the conformations and dynamics of an intrinsically disordered protein. Angew Chem Int Ed Engl. 2021;60(19):10724–10729.
38. Guillaume-Gentil O et al. Tunable single-cell extraction for molecular analyses. Cell. 2016;166(2):506–516.
39. Holmstrom ED et al. Accurate transfer efficiencies, distance distributions, and ensembles of unfolded and intrinsically disordered proteins from single-molecule FRET. Methods Enzymol. 2018;611:287–325.
40. Kong X, Nir E, Hamadani K, Weiss S. Photobleaching pathways in single-molecule FRET experiments. J Am Chem Soc. 2007;129(15):4643–4654.
41. Nir E et al. Shot-noise limited single-molecule FRET histograms: comparison between theory and experiments. J Phys Chem B. 2006;110(44):22103–22124.

Copyright © 2026, Journal of Visualized Experiments
Creative Commons Attribution-NonCommercial-NoDerivs 3.0 Unported License

Materials List for

Microinjection-Based Single-Molecule Fluorescence Spectroscopy: Probing Protein Conformations and Dynamics in Live Cells

Yuhan Wang[1], **Daniel Nettels**[1], **Benjamin Schuler**[1,2]

[1]Department of Biochemistry, University of Zurich [2]Department of Physics, University of Zurich

Corresponding Authors

Yuhan Wang
y.wang@bioc.uzh.ch

Benjamin Schuler
schuler@bioc.uzh.ch

Citation

Wang, Y., Nettels, D., Schuler, B. Microinjection-Based Single-Molecule Fluorescence Spectroscopy: Probing Protein Conformations and Dynamics in Live Cells. *J. Vis. Exp.* (237), e74404, doi:10.3791/74404 (2026).

Date Published

November 20, 2026

DOI

10.3791/74404

URL

jove.com/video/74404

Materials

Name	Company	Catalog Number	Comments
515-nm continuous-wave laser	Omicron	QuixX515-80PS	Used for continuous-wave ALEX excitation.
60× water-immersion objective	Olympus	UPlanApo 60×/1.20 W	60× magnification; numerical aperture 1.20; water immersion.
642-nm continuous-wave laser	Omicron	QuixX642-140PS	Used for continuous-wave ALEX excitation.
Acceptor emission filter	Chroma Technology	LP647RU	Long-pass filter for acceptor-channel fluorescence
Biological safety cabinet	Esco		CytoCulture Class II biological safety cabinet.
CF660R maleimide	Sigma-Aldrich		Acceptor fluorophore; legacy stock.
CO_2 incubator	BINDER	C150; article no. 9140-0078	Humidified incubator operated at 37 °C and 5% CO_2.
Custom-built confocal microscope	Custom-built; Olympus	IX71	Custom-built confocal microscope based on an Olympus IX71 microscope body.
Cy3B maleimide	Cytiva		Donor fluorophore; legacy stock.
Cy3B- and CF660R-labeled prothymosin α (ProTα)	Prepared in-house		Fluorescently labeled protein used for the representative measurements.
Donor emission filter	Chroma Technology	ET585/65m	Band-pass filter for donor-channel fluorescence
Fetal bovine serum	Sigma-Aldrich	F7524-500ML	Cell-culture supplement.
Fluorescence detectors	PerkinElmer	SPCM-AQR-15	Four single-photon counting modules connected to the photon-counting hardware.
FluoroBrite DMEM	Gibco	A1896701	Phenol-red-free cell-culture medium.
Fretica	Schuler Lab		Mathematica add-on for single-molecule fluorescence analysis; https://github.com/SchulerLab/Fretica

Copyright © 2026 JoVE Creative Commons Attribution-NonCommercial-NoDerivs 3.0 Unported License

Glass-bottom imaging dish	ibidi	81158-IBI	µ-Dish 35 mm, high Glass Bottom.
GlutaMAX Supplement	Gibco	35050061	Cell-culture supplement.
Hanks' balanced salt solution (HBSS), modified, with Ca^{2+}/Mg^{2+}	Gibco	14065-056	10× HBSS containing Ca^{2+} and Mg^{2+} and without sodium bicarbonate.
Hanks' balanced salt solution (HBSS), modified, without Ca^{2+}/ Mg^{2+}	Sigma-Aldrich	H6648-500ML	Used to prepare the microinjection solution.
HeLa cell line	ATCC	CCL-2	Human cervical epithelial cell line.
Laser power meter and sensor	Thorlabs	PM400; S120C	PM400 console with S120C sensor (400–1100 nm; maximum power 50 mW).
Microinjection capillaries	Eppendorf (Calibre Scientific)	EPE-5242952008	Femtotips microinjection capillaries.
Microinjection capillary holder/injector	Home-built		Used to mount the capillary and connect it to the pressure controller.
Microinjection pressure and injection-time controller	Home-built		Controls injection pressure and pulse duration.
Microloader tips	Eppendorf (Calibre Scientific)	EPE-5242956003	100-mm Microloader tips used to load microinjection capillaries.
Microscope-stage dish holder	Home-built		Holds the 35-mm imaging dish on the microscope stage.
Penicillin–streptomycin	BioConcept	4-01F00-H	Cell-culture supplement; lot TJ04609P.
Phosphate-buffered saline	BioConcept	3-05F39-I	Used for washing cells during culture.
Pulsed excitation source	NKT Photonics	XW-12	SuperK Extreme pulsed supercontinuum laser used for PIE and fluorescence-lifetime measurements.
Sodium hydroxide	Sigma-Aldrich		Used for pH adjustment; EC no. 215-185-5; lot 23L084105.
SymPhoTime 64	PicoQuant		Software used for photon-data acquisition.
T25 cell-culture flasks with filter caps	Sarstedt	83.3910.002	Used for routine maintenance of HeLa cells.
Time-correlated single-photon counting and time-tagging module	PicoQuant	HydraHarp 400	Four input channels used for photon counting and time-tagged data recording.
Trypsin–EDTA solution, 0.5% (10×)	Sigma-Aldrich/Merck	T4174-20ML	Diluted to a working trypsin concentration of 0.05%.
Tween 20	Calbiochem	655204	Added to the microinjection solution at 0.005% (v/v).
Wolfram Mathematica	Wolfram Research		Version 15; used with Fretica for data analysis.
XenoWorks micromanipulator and joystick	Sutter Instrument		Used to hold and position the home-built microinjection assembly.

Copyright © 2026 JoVE Creative Commons Attribution-NonCommercial-NoDerivs 3.0 Unported License